Neuron, Volume *61*

Supplemental Data

Neural Encoding of Rapidly Fluctuating Odors

Maria N. Geffen, Bede M. Broome, Gilles Laurent, and Markus Meister

Electric Nose Measurements

To measure the dynamics of odor concentration delivered by our apparatus, we constructed a sensor that mimicked the slender shape of the locust antenna. A thin glass capillary (Warner Instrument Corp.) was coated with a film of doped polymer (mixture of carbon black, polyethylene vinyl di-acetate and resin) using an airbrush and established protocols (Matzger, A. J., Lawrence, C. E., Grubbs, R. H., and Lewis, N. S. 2000. Combinatorial approaches to the synthesis of vapor detector arrays for use in an electronic nose. J Comb Chem 2, 301-304). Electrical contacts were made on either side of a 3 mm exposed patch of polymer by attaching copper wires to the glass with silver paint. At baseline, the electrical resistance ranged between 50 kOhms and 500 kOhms. Exposure to vapor increased the resistance. Recordings with this sensor showed that the odor concentration can be rapidly switched on and off every 100 ms. The timing of successive odor pulses was highly reproducible: the delay between valve opening and half-maximal rise of the odor pulse varied by only 0.7 ms (SD). This indicates that the odor can indeed be modulated rapidly and reliably, and over a wide range of concentration (Fig 1E).

In all our reported analyses, the stimulus is the binary state of the solenoid valve in the odor injector line. We considered using the signal from the electric odor sensor, but rejected it for the following reasons. First, the detailed waveform reported by these electric sensors varied considerably among different devices. Second, when we did perform some L-N model fits of neural responses starting from the sensor output, they were less successful than L-N fits starting from the valve signal; they required more convoluted and acausal filter waveforms; and they depended on the device used. These observations suggest that the polymer sensor introduced significant dynamics and distortion in the reported signal. While the sensors served to confirm that odor modulation is rapid and reproducible across trials, they need to be engineered further to provide a quantitative record of odor concentration. In evaluating the reported filter shapes $F(t)$, one therefore needs to recall that these include a brief delay of <0.1 s from valve opening to odor

onset. This air-flow delay is short compared to the neural response delays, and it is identical for all neurons in the sample.

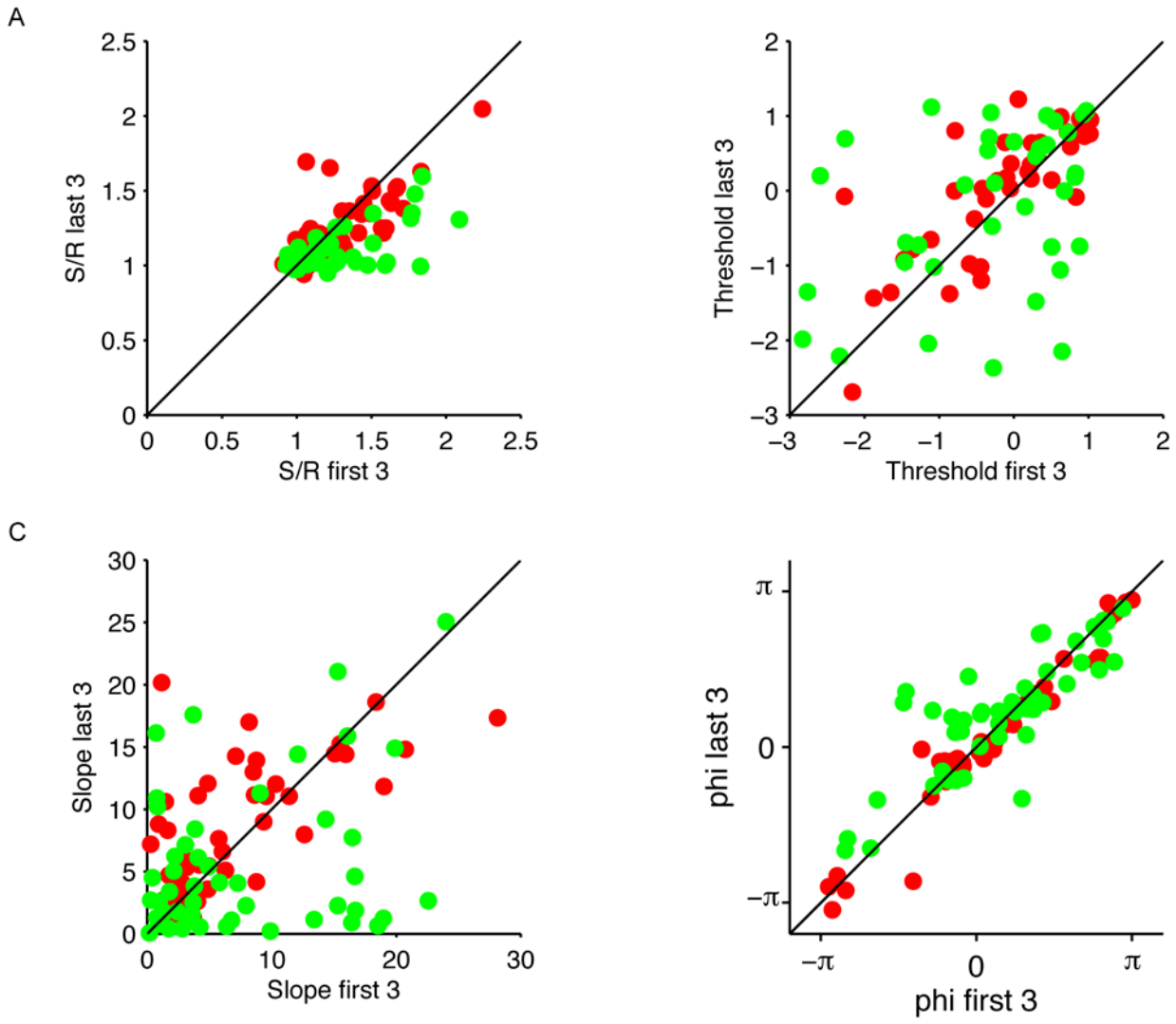

Figure S1. Change in L-N Fits across Trials

Some PNs showed a systematic change in firing rate over the ten trials (Fig 1G). Here we evaluate what aspects of the odor response change during this period. The 3-parameter L-N model (Eqns 7-9) was fit to the first 3 trials and again to the last 3 trials. Analysis included 48 PNs each with reliable responses in the Oct, Hex, and Oct/Hex conditions (Fig 3).

A. The ratio Signal/Residual ($\sqrt{P_S/P_R}$, see Experimental Procedures) compared in early and late trials. Line is the identity. By this measure, the goodness-of-fit is comparable in early and late trials.

B. The threshold of the nonlinearity (Eqn 7) compared in early and late trials. On average, thresholds increase somewhat in late trials.

C. The slope of the nonlinearity (Eqn 7) compared in early and late trials. This parameter reflects the gain of the response and changes considerably between early and late trials, increasing for some PNs and decreasing for others.

D. The shape of the filter compared in early and late trials, as summarized by the shape parameter ϕ (Eqn 8). Note that the filter shape remains essentially the same throughout all trials.

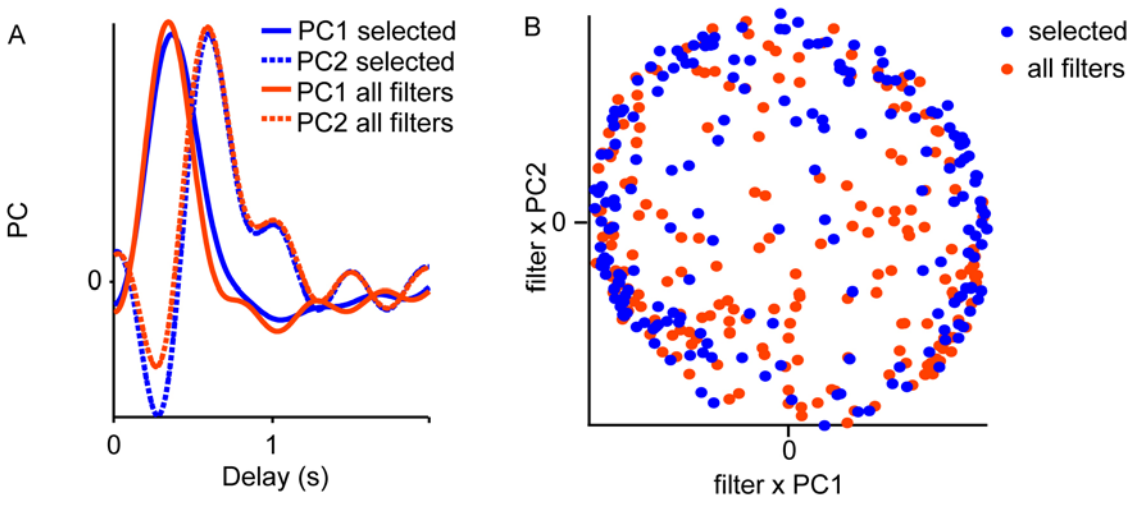

Figure S2. Principal Component Analysis of All Filter Waveforms

The analysis of Figure 4 was restricted to the PNs with the most reliable odor responses, selected as the top 50% in terms of Signal/Noise ($\sqrt{P_S/P_N}$, see Fig 3). Here we test whether the excluded cell/odor combinations with weaker responses had some systematically different kinetics, by repeating the analysis of filter shapes over all neurons. We found no evidence for additional kinetic components.

A. The first two principal components of the filter shapes, computed either for the selected 48 strong responses (same as Fig 4A) or for all 97 responses. No systematic difference is discernable.

B. The filter shapes projected onto the first two principal components, PC1 and PC2 from panel A. The selected filters for strong responses lie close to the unit circle (same as Fig 4B), because these two components account for most of their variance. The excluded filters for weak responses fill more of the space within the circle, because they are corrupted by noise with random waveform other than PC1 and PC2. The fact that PC1 and PC2 are virtually identical to those of the strong responses (panel A) confirms that this noise has no systematic component.

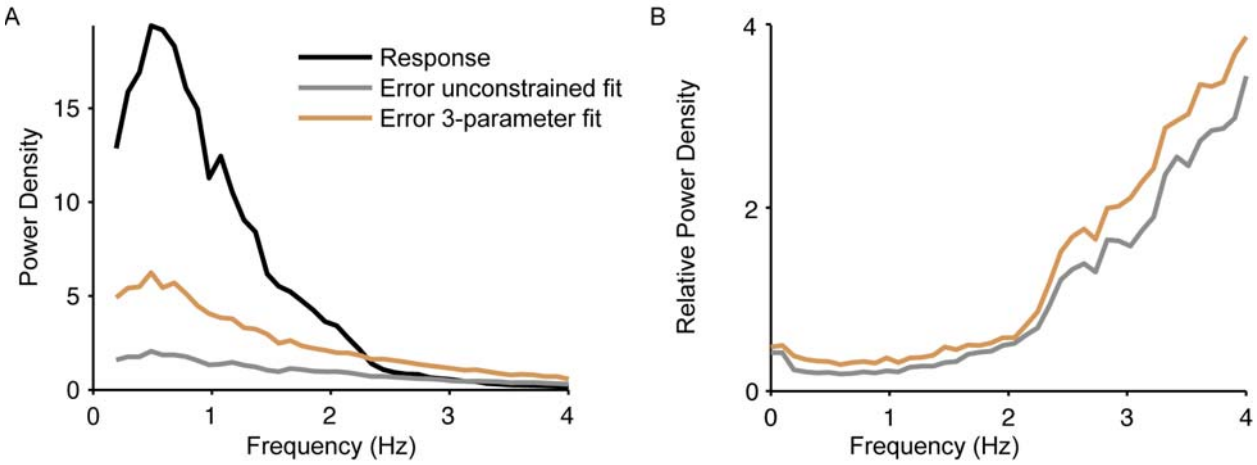

Figure S3. Frequency-Dependence of the 3-Parameter L-N Model Fits

For most cell-odor combinations, the 3-parameter L-N model fits almost as well as the unconstrained L-N model (Fig 4I). On average there is a small loss in fit quality, more so for some cells in the Oct condition. Here we explore the nature of these losses. In particular, one might worry that the 3-parameter model fails at high frequencies, because the waveform of the filter function was approximated by just 2 principal components with rather smooth waveform (Fig 4A). This concern was not validated.

A. Power spectrum of the response $r(t)$ (see Eqn 1), the residual $r'(t) - r(t)$ from the unconstrained L-N fit, and the residual from the 3-parameter fit. Results were averaged over all 48 selected cells (Fig 3) in the Oct condition.

B. Power of the two residuals plotted as a fraction of the power in the response. Note the two residuals have very similar frequency dependence.